**Aberystwyth University**

*Leafless roughness of complex tree morphology using terrestrial LiDAR*
Antonarakis, A. S.; Richards, Keith S.; Bithell, Mike; Brasington, James

# Leafless roughness of complex tree morphology using terrestrial lidar

A. S. Antonarakis,[1] K. S. Richards,[2] J. Brasington,[3] and M. Bithell[2]

[1] Strategies for extracting roughness parameters from riparian forests need to address the issue that the trees are more than just stems and that in large rivers flow can rise into the canopy. Remote sensing information with 3-D capabilities such as lidar can be used to extract information on trees. However, first and last pulse airborne lidar data are insufficient to characterize the complex vertical structure of vegetation because by definition, there are few data at intermediate levels. Terrestrial laser scanning (TLS) is used in this study to define complex structures at a millimetric scanning resolution for the purpose of extracting canopy parameters relevant for the parameterization of the flow resistance equations. We will mainly be concerned with the projected area of leafless trees, estimating the total tree dimensions using several different methods. These include manipulating mass point cloud data obtained from TLS to create stage-dependent projected areas through complex meshing techniques and voxelization. Stage-dependent projected areas were defined for natural and planted poplar forests in the riparian zone of the Garonne and Allier rivers in southern and central France, respectively. Roughness values for planted poplar forests dominant in many western European river floodplains range from Manning's $n = 0.037-0.094$ and $n = 0.140-0.330$ for below-canopy flow (2 m) and extreme in-canopy flow (8 m), respectively. Roughness values for natural poplar forests ranged from $n = 0.066-0.210$ and $n = 0.202-0.720$ for below-canopy flow (2 m) and extreme in-canopy flow (8 m), respectively.

## 1. Introduction

[2] Determining the roughness of vegetation, and especially trees, with different structural characteristics, is needed for use in resistance equations and in flood modeling exercises. Remote sensing information with 3-D data capabilities such as lidar can be used to extract information on trees. Airborne lidar has been used in a previous study [*Antonarakis et al.*, 2008a] to extract simple trunk roughness information relevant to below-canopy flow. Strategies for extracting roughness parameters must also address the issue that trees are more than just stems, and that in larger rivers the flow can rise into the canopy, so further consideration is needed of the resistance of canopies. The consideration of the canopy structure is important not only when the flood stage is high, but also for natural riparian vegetation where the canopy starts relatively near the ground.

[3] It is important to know how to extract hydraulically relevant canopy structure information, and to consider the appropriate scale of technology. Airborne lidar first and last pulse data can be used to examine the vertical structure of selected forest sections and a map of the variation of hits within the different spatial areas can be produced (as with *Antonarakis et al.* [2008b]). However, first and last pulse airborne lidar data are insufficient to characterize the complex vertical structure of vegetation, because by definition, there are few data at intermediate levels. Therefore, a more detailed lidar technique must be used.

[4] Terrestrial laser scanning is used in this study to define complex canopy structures at a millimetric scanning resolution for the purpose of extracting canopy parameters relevant for the parameterization of the resistance equations. Because of power of the scanning technique and the data retrieved, resistance will be calculated for the full submergence of the represented forests types, although resistance equations have not yet been validated for these magnitudes of events. The resulting friction values obtained from terrestrial laser scanning (TLS) methods will first be compared to a recent method developed by *Järvelä* [2004] where the complex canopy structure of forests is defined using branching relationships. *Järvelä's* [2004] method is considered useful as a reference because it is considered as a novel procedure which allows the determination of the friction factor *f* or Manning's *n* using the measurable vegetation structure in terms of its obstacle to water flow. The vegetation structure has previously been incorporated into resistance equations using metrics that are difficult to define in the field (such as momentum absorbing areas), while *Järvelä's* [2004] study offers the possibility of resis-

[1]Department of Organismic and Evolutionary Biology, Harvard University, Cambridge, Massachusetts, USA.
[2]Department of Geography, University of Cambridge, Cambridge, UK.
[3]Institute of Geography and Earth Sciences, University of Wales, Aberystwyth, UK.

**Table 1.** Performance Characteristics of the Leica System TLS[a]

| Characteristics | Leica Geosystems TLS |
| --- | --- |
| Applicable scan range | 0.5–300 m |
| Applicable target range | up to 100 m |
| Scan density maximum | 1.2 mm at 10 m |
| Scan density minimum | selectable |
| Scan speed | 1–3 kHz |
| Data volume | XX-large |
| Point accuracy | 2–4 mm |
| Accuracy at maximum range | 4–10 mm |
| Field of view | 360° × 270° (horizontal/vertical) |
| Spot size | 6 mm at 50 m |

[a]Adapted from *Frei et al.* [2005].

tance calculated from vegetation just through its area that comes into contact with floodwater.

[5] In this paper, we compare the roughness values from the different methods with each other, and in the absence of other control data sets, with values set out in guideline literature. Section 2 briefly describe the terrestrial laser scanning technique and the field sites where data were collected, and in section 3 the resistance equation defining roughness for woody vegetation is explained. Various methods are identified and compared in order to develop extraction techniques from ground scanning information so as to obtain a representative roughness for leafless trees. The first method described in section 4, uses *Järvelä*'s [2004] total projected area calculations, based on branching ratios and lengths determined in the field, assuming a linear distribution of projected area with height. This is then compared, in section 5, to direct extractions of projected areas from ground scans, using as complex meshing and voxelization of lidar point clouds [e.g., *Gorte and Winterhalder*, 2004]. We finally convert the resulting friction values obtained from the methods previously defined to Manning's roughness coefficients in section 6, and represent the values with an increase in potential flow depth for a number of different forest patches.

## 2. Terrestrial Laser Scanning and Study Areas

### 2.1. Brief Introduction to Scanning

[6] Terrestrial-based laser scanning (TLS) is a new technology with the power to rapidly extract extremely dense spatial data. This technique is also an accurate way of capturing the size, shape and form of a complex physical reality. New software allows efficient management of huge data sets in a fully 3-D interactive mode. The capability of TLS to handle large data sets is complemented by its power to combine or register multiple point clouds in a specified area. Thus a three-dimensional region can be fully or almost fully covered from multiple angles, correcting for shadow effects. This research used a Leica Geosystems high-definition surveyor (HDS 3000 scanner head) collecting point clouds and modeling them for analysis using the Cyclone 5.5 software.

[7] Terrestrial laser scanning with this instrument has the capability to collect point cloud data at a maximum distance of 300 m and with a maximum scan density of 1.2 mm at a distance of around 10 m [*Frei et al.*, 2005]. The positioning

accuracy of this data set can be as good as 2–6 mm at proximate ranges, and 10 mm at maximum distances. The performance characteristics of the ground scanner used in this study are shown in Table 1.

[8] If the location and orientation of the scanner are known, then the resulting point cloud data can be registered to any given coordinate system with a millimetric to centimetric accuracy. The steps in collecting TLS data first involve the set up of the scanner in the desired area, along with a number of targets, which are surveyed into an external coordinate system using a total station. Multiple data sets are recorded by placing the scanner in a sufficient number of different locations to ensure good coverage of the objects for which data is needed, with each scan including a subset of the targets. The latter then define a reference frame that allows the separate scans to be combined and then related to a geodetic coordinate system. Further information on data acquisition of HDS scanners is provided by *Frei et al.* [2005].

### 2.2. Scanning Sites

[9] Roughness of forested vegetation is considered in three meanders, the first two being from the heavily managed Garonne River, and the second from the almost unmanaged Allier River. The first two meanders considered were near the village of Verdun-sur-Garonne (UTM31; 359500E, 4854000N), and the second near the village of Monbequi (UTM31; 356000E, 4861500N). The Garonne floodplain consists of a large proportion of commercial planted poplar clones of all ages, which are heavily pruned. Vegetation on the meanders mainly includes natural black poplar (*Populus nigra*), which can be very dense. These are situated on the immediate bank of the river. A secondary natural species was white willow (*Salix alba*), but its distribution was limited [*Muller et al.*, 2002]. One meander section was examined on the Allier near the village of Châtel-de-Neuvre (UTM31; 525250E, 5140350N). Here, most of the surface was bare and consisted of bar forms with variously sized gravel but also sparsely vegetated areas. The main species was again *Populus nigra*.

[10] Leafless roughness was considered for six forest land cover types, four from the Garonne River and two from the Allier River. These included young (VY), intermediate (VI), and mature (VM) planted poplars at the Verdun meander as well as mature natural poplar (Mnb) at the Monbequi meander of the Garonne, and young (ChY) and mature (ChM) planted poplar for the Chatel meander of the Allier. Two types of natural forest were considered, as their density and structure was different resulting from two different river management practices. In June 2006, field data were collected from each of these sites, which included the individual diameter at breast height, trunk height, total tree height, and crown dimensions.

[11] Using TLS, three forest sites were scanned on the Garonne and Allier reaches in February 2007. These were scans of two mature planted poplars at Verdun, and both a mature and young natural poplar at the Chatel meander on the Allier. Scans of younger planted poplar trees were not possible in this winter campaign, as all trees had been severely pruned since collecting ground information in June 2006. Scanning was attempted at the Monbequi site, but

weather conditions did not allow for scan data with a good representation of natural poplars in the winter.

[12] At each site chosen, multiple scans were performed in order to have the maximum 3-D representation of the woody vegetation, while allowing shadowing of the branches and the trunk. For scanning of the branch structure of individual trees, three positions were considered sufficient. Resolutions of 2 cm at the distance from the scanner to the tree trunk were chosen for all trees in order to recover data from small twigs of only a few centimeters in diameter and length.

## 3. Flow Resistance Equation

[13] The roughness of woody vegetation becomes more complex when considering flow that could potentially enter the canopy layers, either with or without their leaves. For simplicity it is assumed that total woody vegetation areas, normal to the flow direction, can be considered constant; that is, the structure does not deform with flow as it is not fully submerged [*Pasche and Rouvé*, 1985]. This assumption simplifies the description of canopy structure, and the determination of its frontal area.

[14] The friction factor of woody vegetation can be characterized by [*Järvelä*, 2004]

$$f = \frac{4A_p(h)}{a_x a_y} C_d \qquad (1)$$

Longitudinal ($a_x$) and lateral ($a_y$) distances are the average spacing between individual tree elements in a forest stand. Friction is associated with a reference area that causes blockage to fluid flow. This is usually represented as the typical area projected on a perpendicular plane in the flow direction. The projected area ($A_p$) in this case is thus a representative tree frontal area typically found in a stand of related characteristics, and is only relevant up until the level of submergence. Branches can constitute a very large proportion of the total leafless tree projected area, and details of their structure are crucial in best describing the resistance associated with a certain forested stand. In theory, bark frontal area as a function of height is needed, which is specific to the tree species and forest type. Different species and forest stands will have a wide variation of cumulative projected area with increase in flow depth, thus the projected area is defined as a function of height ($A_p(h)$).

[15] The drag coefficient ($C_d$) is also included in equation (1). Standard values have been recommended for branched and leafless vegetation of between $C_d = 1-1.5$ [*Järvelä*, 2004]. It has been suggested by *Ishikawa et al.* [2006], though, that true values may diverge from this because of the flexibility and permeability of the tree and its branches. It is desirable then to attempt a semiempirical method to derive the drag coefficient using equation (1). This involves the estimation of the drag force, in order to relate the drag coefficient to the shape and area of the vegetation element directly. *Wu et al.* [1999] described the need to determine the *vegetation drag coefficient* ($C'_d$) that relates the full vegetation projected area $A_{p,tot}$ (i.e., the reference projected area of the fully submerged tree) to the vegetation area per unit volume ($\lambda$: where $V$ is the total volume occupied by the canopy), resulting in the equation

$$C'_d = \frac{2F'_D}{\rho U^2 \lambda} \quad \text{where} \quad \lambda = \frac{A_{p,tot}}{V} \qquad (2)$$

*Lee et al.* [2004] related the vegetation drag force ($F'_D$) to flow parameters including the Reynolds number using fieldwork and modeling, and derived the regression equation for drag force:

$$F'_D = K_o \left( \frac{\rho U^2}{s} \right) R_h^{-k} \qquad (3)$$

In the above equation, $K_o$ is the multiple regression constant, $R_h$ is the Reynolds number based on flow depth, $s$ is the average spacing between vegetation elements, and the exponent ($k$) is another regression coefficient developed by *Tsihrintzis* [2001] which ranges from 0.6 for increasing vegetation frontal area with depth to 1.5 for decreasing frontal area with depth. Relating equations (2) and (3), the drag force can finally be calculated as

$$C_d = \frac{2K_o R_h^{-k} V}{A_{p,tot} s} \qquad (4)$$

According to *Lee et al.* [2004] when flows become turbulent ($R_h = 10,000$) the product of the two variables $K_o R_h^{-k}$ can be assumed to be $0.15-0.2$. We now proceed to calculate projected areas first by using the branching method defined by *Järvelä* [2004], then by using measurements obtained using TLS.

## 4. Total Projected Area Using Branching Ratios

### 4.1. Summary of Branching Method

[16] A method to determine the projected area of leafless trees was developed by *Järvelä* [2004] on the basis of work by *McMahon and Kronauer* [1976] who took the stream-order scheme of Strahler developed in 1956, and applied it to tree branching. *Strahler*'s [1956] study was an important foundation for understanding and defining river systems and their changes, and has subsequently been applied to many other scientific disciplines including allometry and vegetation relationships. The ordering system begins from the smallest branches leading toward the base of the trunk and involves three rules. First the smallest branches are designated with an order of 1. Second the junction of two branches of order "$m$" forms a branch segment of order $m+1$. Third the junction of two branches of unequal order creates a segment having an order equal to that of the higher-order branch (Figure 1). *McMahon and Kronauer* [1976] explained that the branching patterns within any tree species are self-similar with any segment of the tree being a model of the entire tree. They also concluded that for branches or beams that are elastically similar, their diameter proved to be proportional to the 3/2 power of their length, and the ratio of branch numbers proportional to twice its diameter ratio. The three relationships are

$$R_B = \frac{N_m}{N_{m+1}} \qquad (5)$$
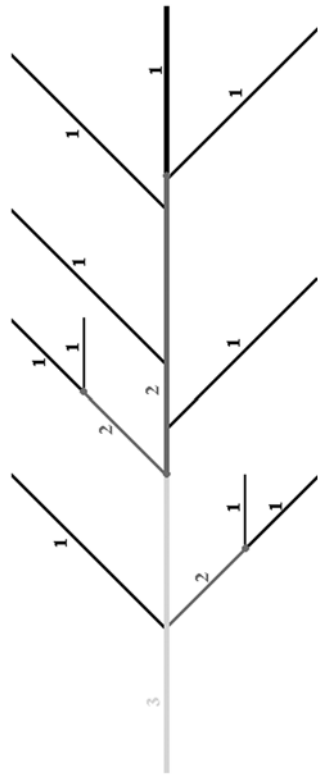
**Figure 1.** The principle of the Strahler ordering scheme applied to a branch from the mature planted poplars. The nodes between the numbered branch orders are shown as dots. Because the total orders are usually unknown, the highest-order branch (trunk) is usually defined as $m$.

$$R_D = \frac{d_{m+1}}{d_m} \approx \frac{1}{2} R_B \qquad (6)$$

$$R_L = \frac{L_{m+1}}{L_m} \approx R_D^{2/3} \qquad (7)$$

In the above equations "$N$" is the number of segments in a particular order (subscript $m$), "$d$" is the average diameter within an order, and "$L$" is the average length within an order. $R_B$ describes how many smaller branches its immediate larger branch can support. Correspondingly, $R_D$ and $R_L$ are branch thickness and length ratios, respectively.

[17] To compute the total projected area of a branched tree ($A_{p,tot}$), seven factors have to be considered and these have to be obtained according to the specific tree structures investigated. These factors are $R_B$, $R_D$, $R_L$, $d_{\min}$ (average diameter of branches of order 1), $d_{\text{high}}$ (average diameter of the highest order, or the trunk), $H$ (plant height), and $L_{\text{high}}$ (length of the highest order). The last three factors can easily be determined in the field. Also, the number of segments in the highest order, $N_{m,\text{high}}$ (number of trunks), need to be assigned. A number of steps presented by *Järvelä* [2004] result in the computation of the total projected area of a branched plant ($A_{p,tot}$), and thus will not be described here. These involve iterative calculations of the number of branche        tree through applying the

branch diameter ratios on the initial trunk diameter until the last-order twigs match the $d_{\min}$ measurement.

### 4.2. Field-Derived Branch Information

[18] The branching ratios developed in this study were obtained from a mature planted poplar at the Verdun site. This type of tree was chosen as it was relatively free growing, had not been pruned for at least 3–4 years, and was a good example of a mature poplar with many branching orders. It was also chosen because there was the possibility of cutting it down and performing measurements on its parts. It should be noted also that tree structures of the same species are assumed to be self-similar, and so one branching ratio and one diameter ratio is enough information for a whole tree (as stated by *McMahon and Kronauer* [1976]).

[19] In the month of June 2007 a mature planted poplar with trunk position UTM31 coordinates 359792.229E, 4853965.888N was felled. According to the theory set out above, diameter and length measurements were made on 22 primary branches (spanning out from the trunk), 57 secondary branches (spanning out from the main branches), and 155 tertiary branches. Once the branching orders had been classified, and the lengths and diameters of all branches had been established, the ratios could be calculated. The final values obtained were $R_D$ = 1.682, $R_L$ = 1.406, and $R_B$ calculated to 3.364. The average measurements for each order are presented in Table 2. The relationship between the branch diameter and length ratios here matches equation (7) where the $R_L$ value of 1.406 is around the 2/3 power of the $R_B$ value of 1.682. The average diameter of the smallest branches belonging to the first order was measured roughly to have been around 1 cm.

[20] The branching ratios determined from this method at first glance are lower than the ratios defined for a number of trees by *McMahon and Kronauer* [1976]. In their study, six trees species were measured with an average $R_D$ of 1.87 and $R_B$ of 4.35. Other research has been done to report branching ratio values with a couple of them provided here. *Oohata and Shidei* [1971] found that in the deciduous trees they considered, the bifurcation ratio ($R_B$) was around 3, with a value of 5 for evergreens. *Barker et al.* [1973] defined $R_B$ values of 4.35 and 4.0 for an apple orchard and birch tree, respectively. They also defined $R_D$ values of 1.90 and 1.94 for the same trees. *Fleurant et al.* [2004] worked with Cypress trees and found the length ratio around 1.56 and bifurcation ratio at 4.65. *Steingraeber et al.* [1979] working on naturally growing maples found a bifurcation ratio as low as 3.19. Unfortunately not much information is available for poplar branching ratios, and especially *Populus nigra* and its hybrids.

**Table 2.** Measured Averages of Lengths and Base Diameters of Branches at Each Order Using Direct Poplar Branch Measurements[a]

| Tree Type | Order $m-2$ | | Order $m-1$ | | Order $m$ | |
|---|---|---|---|---|---|---|
| | $L$ | $D$ | $L$ | $D$ | $L$ | $D$ |
| All | 0.204 | 0.0251 | 0.243 | 0.0296 | 0.394 | 0.0647 |

[a]Length is $L$ and base diameter is $D$. Both are given in meters. The order "$m$" starts from the mother branch (i.e., the 22 branches attached to the trunk).

**Table 3.** Initial Branching Parameters for the Six Study Sites[a]

| Site | $N_{m,\text{high}}$ | $d_{\text{high}}$ | $L_{\text{high}}$ |
|---|---|---|---|
| Verdun young poplar | 1 | 0.1113 | 3.796 |
| Verdun intermediate poplar | 1 | 0.1913 | 6.397 |
| Verdun mature poplar | 1 | 0.3474 | 7.66 |
| Monbequi poplar | 2.474 | 0.354 | 4.804 |
| Chatel young poplar | 1.2 | 0.129 | 2.817 |
| Chatel mature poplar | 1.8 | 0.42 | 5.755 |

[a]The diameters and branch lengths are in meters.

[21] It is finally necessary to determine three variables before proceeding in the calculation of the total projected areas of the six major forest sites of this paper. These are the number of trunks in a tree element ($N_{m,\text{high}}$), the average trunk diameter of a stand ($d_{high}$), and the length of the last-order branch (i.e., the trunk: $L_{high}$). All the values were defined in the field for the six study sites, and the information is presented in Table 3.

### 4.3. Total Projected Areas

[22] The iterative process defined fully by *Järvelä* [2004] is finally carried out to estimate the number of branches in an order from the diameters measurements. This is done by using the diameter ratio in equation (6) iteratively until $d_m <$ $d_{min}$ (where $d_{min} = 0.01$ m) starting from the trunk diameter. Then, multiplying $N_m$, $d_m$, and $L_m$ for each order calculates the projected area for that order, and summing these up results in the total projected area ($A_{p,tot}$) calculation. The six sites using the same branching ratios from the first method are presented in the sets of Tables 4a –4f. The stage-dependent projected area or the six forest types were taken to be linear as with the assumption stated by *Järvelä* [2004]. The total projected areas defined in Tables 4a–4f can be compared to those defined using TLS point clouds.

## 5. Stage-Dependent Projected Areas Using Terrestrial Laser Scanning

[23] In this section, stage-dependent projected areas are extracted from terrestrial laser scanning using two methods. The first method creates complex meshes of point cloud data, and the second aggregates point cloud data into equal-sized voxels.

### 5.1. Complex Tree Mesh

#### 5.1.1. Complex Meshing

[24] For our purposes a mesh is a collection of triangular unbroken, nonoverlapping faces joining together along their

**Table 4a.** Derivation of the Total Projected Areas for the Young Planted Poplar Using the First Branching Ratio Method[a]

| | $N$ | $d$ | $L$ | $A_p$ |
|---|---|---|---|---|
| Branching order | | | | |
| $m - 4$ | 128.063 | 0.014 | 0.971 | 1.730 |
| $m - 3$ | 38.069 | 0.023 | 1.366 | 1.216 |
| $m - 2$ | 11.316 | 0.039 | 1.920 | 0.855 |
| $m - 1$ | 3.364 | 0.066 | 2.700 | 0.601 |
| $m$, trunk | 1 | 0.1113 | 3.796 | 0.422 |
| $A_{p,\text{tot}}$ | | | | 4.824 |

[a]The decimals of branch numbers per order are kept to indicate the ratio spanning off from the average trunk numbers. The branch diameters ($d$) and lengths ($L$) at each order are in meters and the projected areas ($A_p$) are in meters squared, while $N$ is the        r of branches in an order.

**Table 4b.** Derivation of the Total Projected Areas Intermediate-Aged Planted Poplar Using the First Branching Ratio Method[a]

| | $N$ | $d$ | $L$ | $A_p$ |
|---|---|---|---|---|
| Branching order | | | | |
| $m - 5$ | 430.804 | 0.014 | 1.164 | 7.127 |
| $m - 4$ | 128.063 | 0.024 | 1.637 | 5.010 |
| $m - 3$ | 38.069 | 0.040 | 2.302 | 3.522 |
| $m - 2$ | 11.316 | 0.068 | 3.236 | 2.476 |
| $m - 1$ | 3.363 | 0.114 | 4.549 | 1.740 |
| $m$, trunk | 1 | 0.1913 | 6.397 | 1.224 |
| $A_{p,\text{tot}}$ | | | | 21.1 |

[a]The decimals of branch numbers per order are kept to indicate the ratio spanning off from the average trunk numbers. The branch diameters ($d$) and lengths ($L$) at each order are in meters and the projected areas ($A_p$) are in meters squared, while $N$ is the number of branches in an order.

three edges [*Remondino*, 2003]. A mesh therefore contains vertex coordinates, edges, and faces, and such a mesh is also sometimes called a triangular irregular network (TIN). Few studies have tried to create meshes or TINs from point cloud data recovered using terrestrial laser scanning, mainly because of the lack of algorithms or programs to perform the meshing. These studies have tried to perform triangulations of point cloud data using Voronoi diagrams and Delauney tetrahedrization, which work on creating polygons around individual points and their nearest neighbors [e.g., *Remondino*, 2003; *Horman and Reimers*, 2004]. *Kim and Li* [2006] have recognized the need to create a complete 3-D surface reconstruction from unstructured and randomly spaced point cloud data. Their work has focused on the need to create an algorithm that connects point clouds, which have a high probability of belonging to one surface form, rather than an adjacent one, therefore reducing jagged edges. Complex meshing can create combined meshes according to the knowledge of the systematic acquisition of the points.

[25] Meshes were automatically created for the four trees scanned in the month of February 2007 using the Leica Cyclone program specific to the Leica laser scanner used in this study. Two Planted poplars in the Garonne were scanned from 3 different positions, and two natural poplars, young and mature, were scanned in the Allier from two to three positions, respectively. Complex meshes of the trees scanned are presented below in Figure 2. A hindrance in creating solid complex meshes of the desired trees was the

**Table 4c.** Derivation of the Total Projected Areas for the Mature Planted Poplar Using the First Branching Ratio Method[a]

| | $N$ | $d$ | $L$ | $A_p$ |
|---|---|---|---|---|
| Branching order | | | | |
| $m - 6$ | 1449.225 | 0.015 | 0.992 | 22.052 |
| $m - 5$ | 430.804 | 0.026 | 1.394 | 15.503 |
| $m - 4$ | 128.063 | 0.043 | 1.960 | 10.898 |
| $m - 3$ | 38.069 | 0.073 | 2.756 | 7.662 |
| $m - 2$ | 11.316 | 0.123 | 3.875 | 5.386 |
| $m - 1$ | 3.364 | 0.207 | 5.448 | 3.786 |
| $m$, trunk | 1 | 0.348 | 7.660 | 2.662 |
| $A_{p,\text{tot}}$ | | | | 67.949 |

[a]The decimals of branch numbers per order are kept to indicate the ratio spanning off from the average trunk numbers. The branch diameters ($d$) and lengths ($L$) at each order are in meters and the projected areas ($A_p$) are in meters squared, while $N$ is the number of branches in an order.

**Table 4d.** Derivation of the Total Projected Areas for the Mature Natural Poplar at the Garonne Using the First Branching Ratio Method[a]

| | $N$ | $d$ | $L$ | $A_p$ |
|---|---|---|---|---|
| Branching order | | | | |
| $m - 6$ | 3585.384 | 0.016 | 0.622 | 34.856 |
| $m - 5$ | 1065.81 | 0.026 | 0.874 | 24.504 |
| $m - 4$ | 316.8281 | 0.044 | 1.229 | 17.226 |
| $m - 3$ | 94.18195 | 0.074 | 1.728 | 12.110 |
| $m - 2$ | 27.99701 | 0.125 | 2.430 | 8.513 |
| $m - 1$ | 8.322536 | 0.210 | 3.417 | 5.985 |
| $m$, trunk | 2.474 | 0.354 | 4.804 | 4.207 |
| $A_{p,tot}$ | | | | 107.401 |

[a]The decimals of branch numbers per order are kept to indicate the ratio spanning off from the average trunk numbers. The branch diameters ($d$) and lengths ($L$) at each order are in meters and the projected areas ($A_p$) are in meters squared, while $N$ is the number of branches in an order.

**Table 4f.** Derivation of the Total Projected Areas for the Mature Natural Poplar at the Allier Using the First Branching Ratio Method[a]

| | $N$ | $d$ | $L$ | $A_p$ |
|---|---|---|---|---|
| Branching order | | | | |
| $m - 6$ | 2434.7 | 0.017 | 0.745 | 30.4 |
| $m - 5$ | 723.751 | 0.028 | 1.047 | 21.4 |
| $m - 4$ | 215.146 | 0.048 | 1.473 | 15.1 |
| $m - 3$ | 63.9554 | 0.081 | 2.071 | 10.7 |
| $m - 2$ | 19.0117 | 0.136 | 2.911 | 7.55 |
| $m - 1$ | 5.65152 | 0.230 | 4.093 | 5.33 |
| $m$, trunk | 1.68 | 0.389 | 5.755 | 3.76 |
| $A_{p,tot}$ | | | | 94.32 |

[a]The decimals of branch numbers per order are kept to indicate the ratio spanning off from the average trunk numbers. The branch diameters ($d$) and lengths ($L$) at each order are in meters and the projected areas ($A_p$) are in meters squared, while $N$ is the number of branches in an order.

effect of the wind while scanning. This would create too many triangles for branches that may have been scanned in multiple positions. Also there is a second hindrance in that laser emissions reflecting off the edge of objects can be recorded as having a false random position. In other words, points that reflect from the edge of a circular object may often be recorded a small distance behind that edge. Thus, a cylindrical branch may return reflections that do not look hemispherical, but u shaped (with the u shape aligned with the direction of the ray from the scanner to the branch). Section 5.1.2 briefly described the full bark areas obtained from complex meshes.

### 5.1.2. Full Bark Areas

[26] After producing the meshes of each of the tree point clouds, each individual triangle mesh is considered, and its area is extracted. All areas are then added up to produce the full bark area of the tress. It is important to remember that the full bark areas are not the projected areas of the trees. The area of each individual triangle was not counted twice; rather the full bark area calculations were due to the multiple scan coverage from different angles. Perhaps then, because we are dealing with floods that theoretically come into contact with one side of the tree (the other side not offering resistance as assumed also by *Järvelä* [2004]), the full bark areas should be halved. Therefore, if the halves of the full areas are taken, then the projected areas are 53.33 m$^2$, 65.86 m$^2$, 69.92 m$^2$, and 5.99 m$^2$ (Table 5). These values are quite similar to the projected areas defined in the branch

ratio method for the two mature planted and young natural poplars, respectively (Tables 4a–4f), except for the mature natural tree at the Chatel meander. The density of the lower canopy, and the height of the tree may have caused some branches higher up in the canopy to have not returned any pulses.

### 5.1.3. Stage-Dependent Bark Areas

[27] The projected areas in different equal vertical segments were also measured to estimate the stage-dependent exposure to the flow. These vertical segments were aided by the elevation values provided with the exported mesh coordinates. Therefore, in addition to exporting the areas of each triangle, their average elevation was also exported. This allowed the subsequent grouping of the triangular faces and calculated areas into a number of defined vertical segments. Figure 3a (section 5.2) shows a graphical illustration of the cumulative projected areas of the investigated trees using the complex meshing method with an increase in height, along with the vertical variations of their projected area in Figure 3b.

[28] The cumulative tree areas with height are important when considering the overall roughness of a vegetated patch with a specific flow depth. It is quite noticeable that the two planted poplars have a surge of bark area above a certain height, which constitutes the end of the single trunk (about 4 m), while the natural poplars in the Allier floodplain have a greater amount of their total area concentrated near the bottom of the tree. This would produce different resistance values, as low flows would come into contact with the complex canopy quicker than for planted poplars. For the young natural poplar, it seems that the canopy starts almost immediately from the ground layer or in the first meter. The young natural poplar in Figure 3a was more linear than the others. This is interesting as it suggests trees in heavy competition with their nearest neighbors will grow in height more rapidly in order to compensate for restrictions on grown in width.

### 5.2. Tree Voxelization

### 5.2.1. Defining Voxels

[29] A voxel, or a volumetric pixel, represents a volume element on a regular grid in the third dimension, instead of the second dimension like the pixel, centered on a coordinate grid point. Each voxel can have a binary or numeric

**Table 4e.** Derivation of the Total Projected Areas for the Young Natural Poplar at the Allier Using the First Branching Ratio Method[a]

| | $N$ | $d$ | $L$ | $A_p$ |
|---|---|---|---|---|
| Branching order | | | | |
| $m - 4$ | 153.676 | 0.016 | 0.721 | 1.785 |
| $m - 3$ | 45.682 | 0.027 | 1.014 | 1.255 |
| $m - 2$ | 13.580 | 0.046 | 1.425 | 0.882 |
| $m - 1$ | 4.037 | 0.077 | 2.004 | 0.620 |
| $m$, trunk | 1.2 | 0.129 | 2.817 | 0.436 |
| $A_{p,tot}$ | | | | 4.979 |

[a]The decimals of branch numbers per order are kept to indicate the ratio spanning off from the average trunk numbers. The branch diameters ($d$) and lengths ($L$) at each order are in meters and the projected areas ($A_p$) are in meters squared, while $N$ is the n    f branches in an order.

**Figure 2.** Images of complex meshes created for (left) a mature planted poplar, (middle) a mature natural poplar, and a (right) young natural poplar. The leafless trees are not drawn to scale.

value associated with it, which can represent some property such as color, density, intensity, elevation, etc. [*Stoker*, 2004]. Voxels are being preferred to other measures because of their insensitivity to the complexity of the object, the ability to import them into simulations, and their ability to allow for different volumes and size. Tree structuring has recently been attempted using voxels on laser scanning data [*Gorte and Pfeifer*, 2004; *Gorte and Winterhalder*, 2004; *Hosoi and Omasa*, 2006]. Using voxels can improve the visualization of woody vegetation, but may also be important in calculations of biomass, crown density, and so on.

[30] *Gorte and Pfeifer* [2004] and *Gorte and Winterhalder* [2004] have processed terrestrial laser scanned points of a tree from multiple scanning positions to a 3-D voxel space. The purpose of this study was to estimate the economic value of forests such as wood volume and straightness of the stem and trees. Voxelizing was performed in these studies by rasterizing the point clouds using 3-D neighborhood operations, and thinning the tree representation to a couple of voxels, and then segregating the branches to eventually obtain their value. *Hosoi and Omasa* [2006] rasterized a registered point cloud data set of a tree in the third dimension, where each individual point represented a voxel with a size relevant to the location of its nearest neighbor.

### 5.2.2. From Point Cloud to Voxel

[31] A method was developed to take the multiple vegetation scans in their point cloud form to a voxel representation. Trees were then visualized on a 2-D plane using ray tracing (in this case with the open source program POV-Ray (www.povray.org)). POV-Ray was chosen as it is a high-definition visual graphics software that can easily be used in order to visualize output from C++ programming. The method deployed here is also explained in the flowchart in Figure 4.

[32] The first step to this algorithm was to define the edges of the 3-D point cloud data set in terms of its maximum and minimum $x,y,z$ points. This then provided the framework for the development of the 3-D grid containers over the incorporated data set. The user defines the size of the grid. Within these 3-D cubic containers, a minimum set of points is defined          points. The reason for this
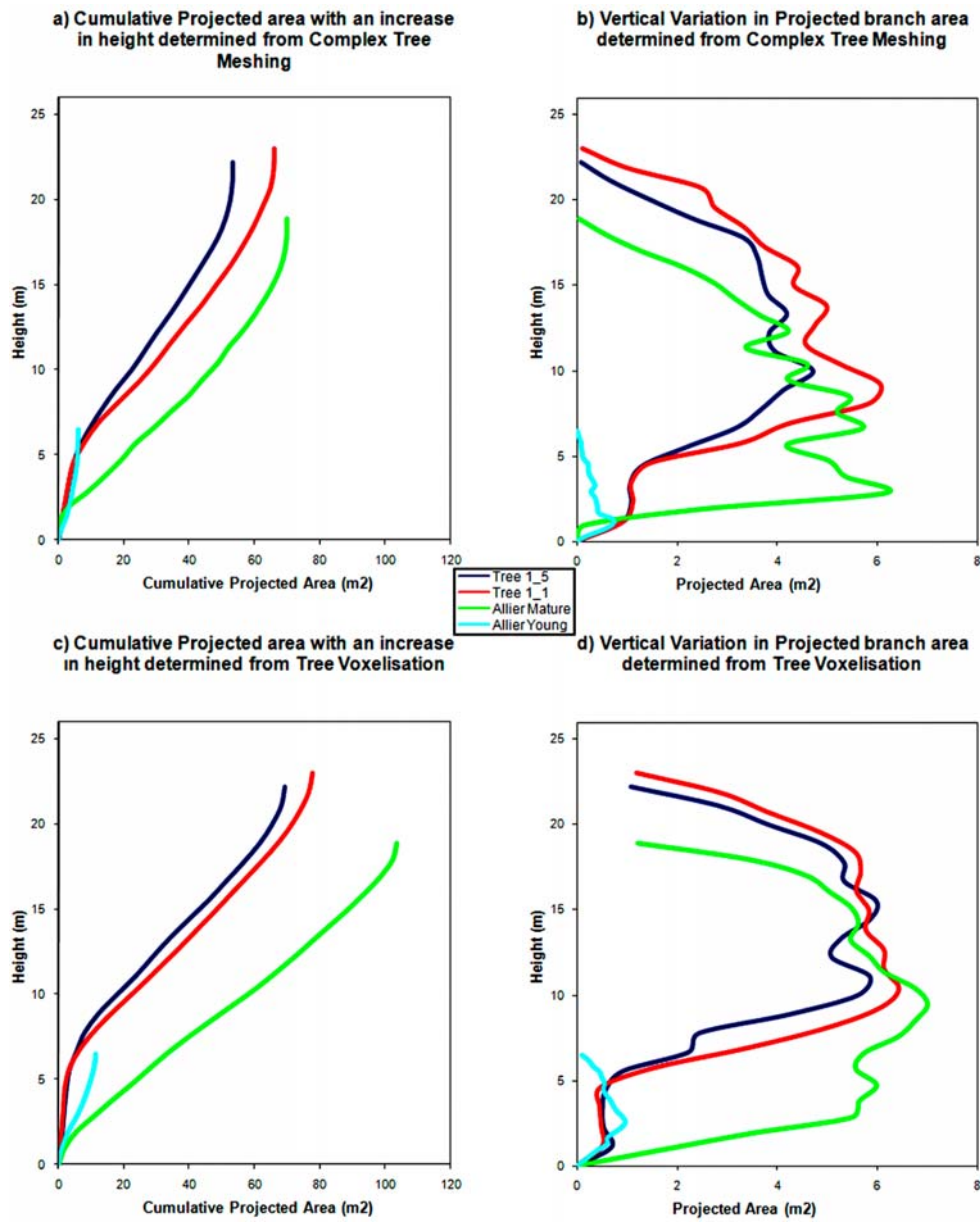
choice was to remove the influence of reflected points off raindrops and other particulate matter. Subsequently for each grid, the upper left hand edge coordinates were defined. The reason for this is that when creating voxels or cubes in the POV-Ray software, it requires the top left edge of each rather than the center. Then when each coordinate has been defined for each grid, it is exported in POV-Ray format with information about the shape (cube) and the color. In other words points that are bucketed into regular 3-D grids have their average point positions established, and are then fed into POV-Ray using its specific format, with a defined coordinate system. For simplicity the coordinate system was set to an arbitrary origin with $x,y,z$ values of 0,0,0 for the top left hand grid cell with point clouds associated with it. The list of voxels created with the relevant information was then output as a text file with a format that was compatible with POV-Ray. Finally, a light source was applied to the visualization interface, and the final voxelized tree was shown. Each of the four trees scanned in the winter are presented with a voxel resolution of 5 cm (Figure 5). The voxel resolution of 5 cm was chosen considering the computational capacity. The C++ program was able to input millions of points, but there was a limit to the number of grids (voxels) that could be created. In fact, the lowest resolution that could output results that could be displayed in POV-Ray was 5 cm, and was a memory rather than a time constriction. This ultimately might introduce

**Table 5.** Projected Area of the Four Trees Scanned in February at the Garonne and Allier Rivers Using the Complex Meshing and Tree Voxel Methods[a]

| | Verdun Mature Planted Poplar 1_5 | Verdun Mature Planted Poplar 1_1 | Chatel Mature Natural Poplar | Chatel Young Natural Poplar |
|---|---|---|---|---|
| Complex meshing method $A_p$ (m²) | 53.33 | 65.86 | 69.92 | 5.99 |
| Voxel method $A_p$ (m²) | 69.171 | 77.74 | 103.541 | 11.167 |

[a]$A_p$, projected area. The mature planted poplar used for determining branching ratios is planted poplar 1_5.

**a) Cumulative Projected area with an increase in height determined from Complex Tree Meshing**

**b) Vertical Variation in Projected branch area determined from Complex Tree Meshing**

Tree 1_5
Tree 1_1
Allier Mature
Allier Young

**c) Cumulative Projected area with an increase in height determined from Tree Voxelisation**

**d) Vertical Variation in Projected branch area determined from Tree Voxelisation**

**Figure 3.** (a and c) Cumulative projected areas and (b and d) stage-dependent projected areas of the four trees considering an increase in flow depth and the two TLS methods of determining projected area (complex meshing and tree voxelization). Tree 1_1 and tree 1_5 are the two mature planted poplars scanned.

errors associated with the total projected area derived from this method compared to the complex meshing method.

### 5.2.3. Stage-Dependent Projected Areas

[33] For estimating the total and stage-dependent projected areas, there needed to be a reference point on the POV-Ray tree visualization with its size being known. Therefore, a visible and recognizable point (red cube) with dimensions of 10 cm was created for each of the tree voxel visualizations. Each image was subsequently exported into a *.jpeg format, and imported into MATLAB. An area extraction algorithm was then applied to the image to create estimates of the total projected area and the stage-dependent projected area. First, the red square was identified from its color intensity, and the number of pixels was found for the square face. Each pixel wa       attributed with an estimated

area. Hence, the total projected area of the leafless trees was the number of nonwhite, nonred pixels in the pixelated image, multiplied by the estimated area for each pixel. Then, the top and bottom rows of the tree were taken, and 20 equal segments were created from them. Finally, each row was attributed with the number of bark pixels, and the estimated bark area. This process was reapplied for four different rotation angles (0°, 20°, 50°, 90°), and the average of each projected areas were taken. Figure 3 illustrates the cumulative (Figure 3c) and stage-dependent (Figure 3d) projected areas determined from this method, and Table 5 states the total projected areas of the four trees investigated.

[34] It is important to notice the similarity in the stage-dependent projected areas (Figure 3d), as well as the cumulative projected areas (Figure 3c), to the projected
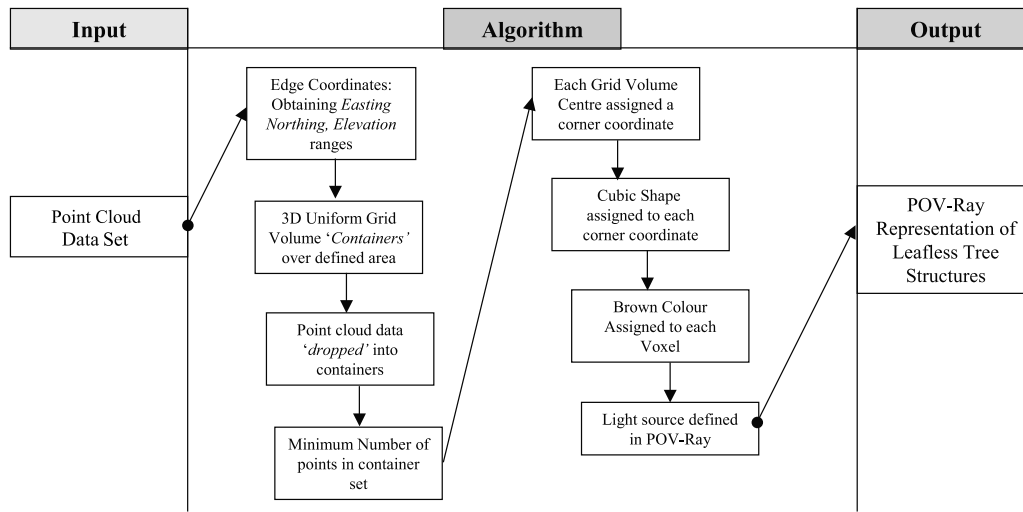
**Figure 4.** Flow process for obtaining voxelized trees represented visually using the C++ program and POV-Ray interface.

areas with height defined by the complex meshing method shown in Figures 3a and 3b. The starkest difference is the younger natural poplar on the Chatel meander on the Allier River. For this method, the stage-dependent projected area is not linearly distributed with a clear increase in bark area in the beginning, and a decrease past $2-3$ m of height. It is also important to notice how similar the total projected areas derived from this method are to the values defined from the Branching Ratio method described earlier in this study. The total projected areas shown in Tables 4a−4f and 6 are very similar, with percentage differences of less that 10% between them. The only exception is for the younger natural poplar tree, which is around twice the value reported (i.e., 11.167 m$^2$ compared with 4.824 m$^2$).

[35] The two main sources of error for this method and for the previous complex meshing method are similar. First and foremost, the wind would affect the number of points being hit and reflected back to the instrument. Therefore, the windier the weather conditions, the more points

reflected from the same surface moving in the wind. This would ultimately result in the projected areas being larger than if the tree was still. This effect was the worst for the young natural poplar on the Allier, so the bark area error associated with this tree would be the largest. Second, for curved surfaces such as branches, the point positions reflected and recorded from the scanner are not always in the correct position. Therefore, there would be tails of points associated with the curved edges of branches, and this would increase the areas of bark. It is difficult to consider a control for these methods, therefore it has been necessary to compare different methods to derive acceptable estimates of both the total projected area, and the stage-dependent projected areas.

## 6. Roughness for Leafless Woody Vegetation

[36] The final objective of this study was to compare the roughness values obtained using the projected areas defined
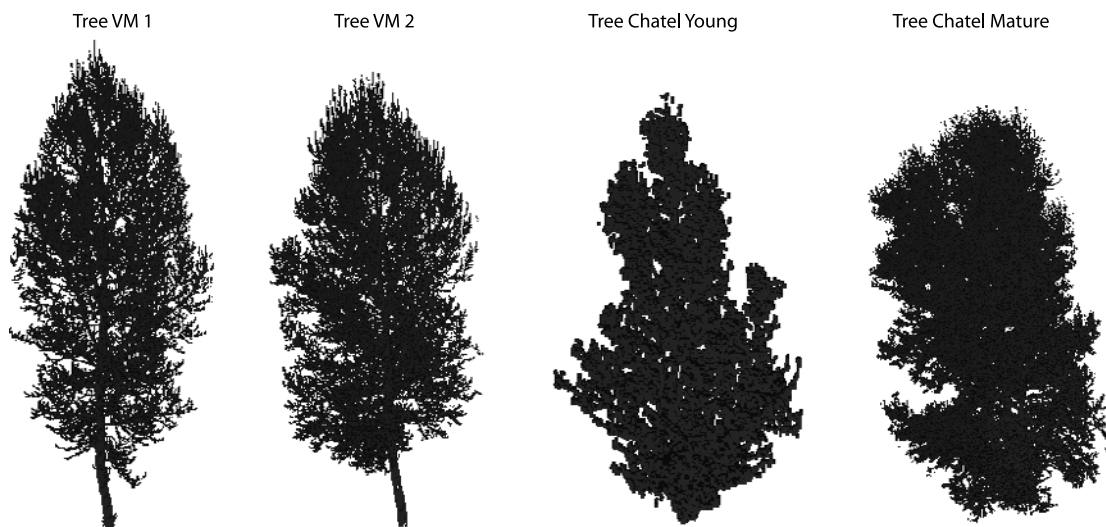


**Figure 5.** Voxelixed leafless trees (not to scale) from POV-Ray. The cells have a resolution of 5 cm. The tree that was fe     as the first mature planted poplar at Verdun (VM 1).

**Table 6.** Drag Coefficients Defined From Equation (4) for the Six Different Sites Considering the Three Methods for Obtaining Total Projected Areas

|  | Branching Method | Complex Meshing | Voxel Method |
|---|---|---|---|
| VY | 1.599 |  |  |
| VI | 1.601 |  |  |
| VM | 1.759 | 2.005 | 1.627 |
| Mnb | 0.304 |  |  |
| ChY | 1.712 | 1.422 | 0.763 |
| ChM | 0.813 | 1.097 | 0.741 |

from the different methods. The stage-dependent projected areas have been defined for the six different poplar stand types, and can now be applied to the resistance equation (1). The drag coefficient $C_d$ is estimated in this research using equation (4). The final resistance values will be obtained for the methods described in this study using terrestrial laser scanning.

### 6.1. Drag Coefficient

[37] It is very difficult to define the drag coefficient of vegetation, and even more difficult if that vegetation is tall and woody in character. Rather than use a standard value, an attempt was made to incorporate projected area measurements into a calculation of the drag coefficient. Equation (4) incorporates the total projected area of leafless tree ($A_{p,tot}$), the volume occupied by the tree ($V$), and the spacing of the individual tree elements ($s$). Using the three methods described in this study, the drag coefficients for the forest sites are shown in Table 6.

[38] The average spacing of the individual elements was taken from the field measurements, and was the product of the average lateral and longitudinal distances between trees. The volume of the individual tree elements was defined as the product of the lateral and longitudinal widths of the crowns and their total height. Around half of the bark drag coefficients obtained were close to the $C_d = 1-1.5$ value, while some of them were far below one (e.g., for Monbequi). Even so, it was thought that the drag coefficient for vegetation elements should take into account the total projected area and aspects of its permeability, as a standard value does not differentiate between different types of trees. Therefore, these values will be used in the roughness calculations illustrated in section 6.2.
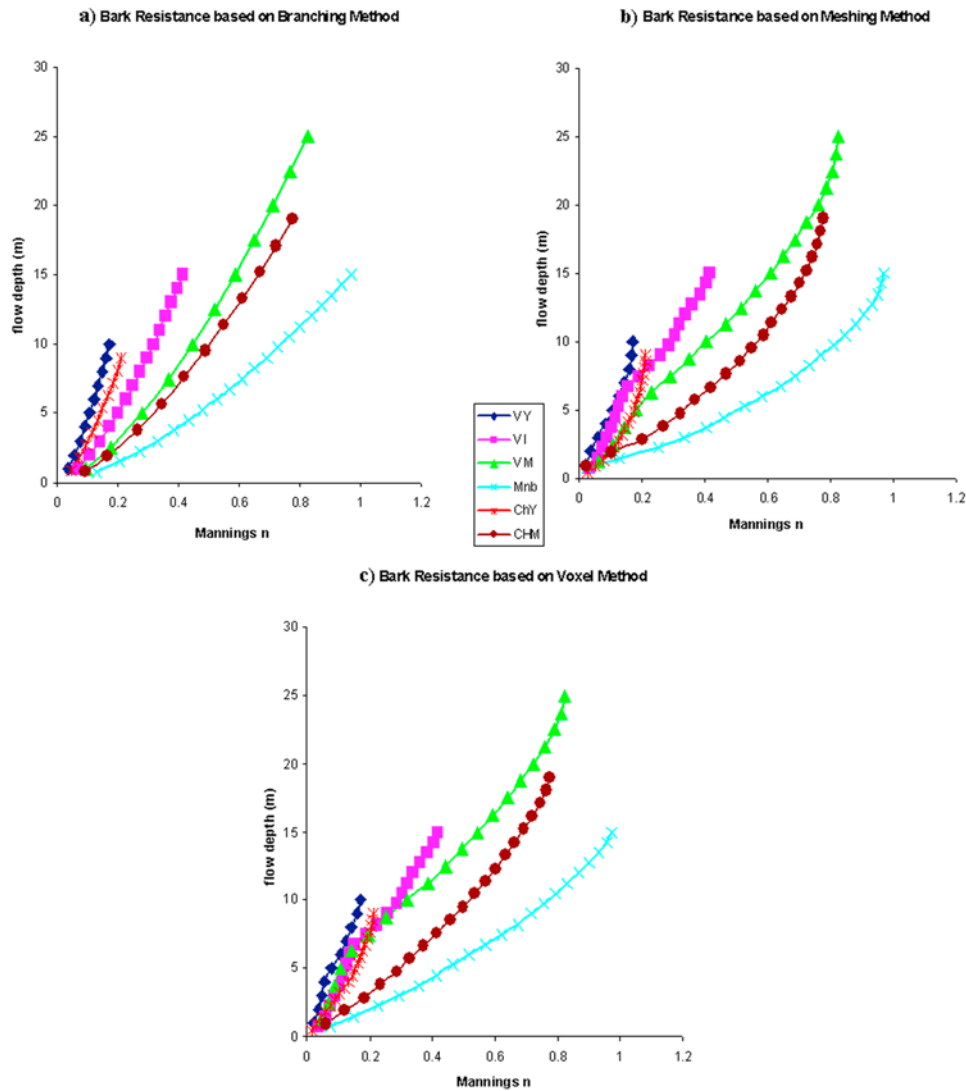
### 6.2. Manning's *n* Values

[39] Resistance values were calculated using equation (1), and Darcy-Weisbach friction factors were then transformed into Manning's *n* values [*Fathi-Maghadam and Kouwen*, 1997]. Stage-dependent projected areas were sometimes inferred for the various methods, where estimations were not available. For the complex meshing and voxel methods, the planted poplars were all related to the mature planted poplar cumulative projected area percentages, while the Monbequi site was related to the mature natural poplar percentages. Final Manning's *n* values with an increase in height until full submergence are presented in Figure 6. It should be noted that estimations of roughness for tall woody vegetation as high as 20 m would involve extreme flooding events, and therefore empirically derived resistance equations may not apply.

[40] The argument for better determining the total and stage-dependent projected areas of floodplain vegetation is reinforced when looking at Figure 6. The larger the tree, the more complex its morphology, and the more heterogeneous its roughness with height. The differences can be determined more closely by comparing the values range of Manning's *n* values at selected flow depths. First, results for the terrestrial scanning methods can be demonstrated at the three flow depths of 2, 4, and 8 m (Table 7). These were selected as the first height corresponded to the upper limit of the trunk for most forest sites; the second height corresponded to water reaching the canopy for the natural poplars; and the third height corresponded to the flow water reaching the canopy for all the poplars.

[41] The roughness values resulting from the branching-order method at 2 m were on average 60% higher for planted poplars, and 20% higher for natural poplars than the values stated above. At 4 m the roughness values were on average 62% higher for planted poplars, but only 3% lower for natural poplars. At 8 m, the values were on average 25% higher for planted poplars, and 11% lower for natural poplars. Therefore at these flow depths it is very important to be able to define the stage-dependent projected area of all types of vegetation. At these lower flow depths, planted forests contain a lower proportion of their total area, while natural forests contain a higher proportion of their total area, compared to the linear average.

[42] There is no independent information to determine how close the values obtained from these three methods are to true roughness coefficients for flow in tree canopies. Therefore it is necessary to compare values to guideline literature such as *Chow* [1959] and the *Arcement and Schneider* [1989]. Some relevant values for flow through riparian forests are shown in Table 8. A couple of other studies have attempted to supply woody vegetation with resistance values, but have focused on leafy vegetation rather than leafless vegetation [e.g., *Kouwen and Fathi-Moghadam*, 2000; *Järvelä*, 2002]. In reality, though, little or no research has measured the roughness of large living forested vegetation especially in the dormant winter period. For example, *Järvelä* [2002] performed flume experiments over willows that were 70 cm tall, and obtained leafless roughness values of $n = 0.038-0.160$. *Coon* [1997] also attempted to determine the roughness of vegetation lined channels with the presence of trees, and stated a winter roughness value of $n = 0.029-0.134$. Keeping these values in mind, the vegetation roughness values obtained in this study are quite similar especially when considering the values presented from *Arcement and Schneider* [1989]. In fact the second last set of values presented in Table 8 considers a flow depth range of up to 2 m. The natural poplar sites at 2 m flow depth present roughness values near the $n = 0.120-0.200$ range ($0.068-0.222$), and the planted poplar sites at 2 m present roughness values near the $n = 0.065-0.140$ range ($0.037-0.113$). Judging from these similarities, vegetation roughness for an increase in flow depth would be acceptable, and the only serious limitation could be the resistance equation at these depths.

[43] A number of studies have attempted to simulate or retrieve the velocity of floodwater in and around woody vegetation, and this kind of information can also be useful in validating the structural and resistance results in this

**Figure 6.** Manning's *n* values for the six sites studied with flow depth until full submergence of all the forest types. The roughness values are presented for (a) the branching and tree model method, (b) the complex meshing method, and (c) the voxel method. The tree types, as defined in section 2.2, are the three ages of planted poplar at Verdun (VY, VI, and VM), the Monbequi natural poplar site (Mnb), and the two different aged natural poplars at Chatel (ChY and ChM).

study, as there was no field data available for riparian flooding in the Garonne and Allier rivers. Normalized velocity distributions were calculated for an increase in the normalized flow depth per forest type, and the results

are shown in Figure 7. The flow depth is normalized by the maximum forest stand height, and the flow velocity is normalized by the calculated maximum velocity around a tree type. The normalized values of flow velocity were chosen for easier comparisons between the TLS methods

**Table 7.** Leafless Manning's *n* Roughness Values for Three Different Flow Depths Considering a Range of Values for All Methods Described in This Study[a]

| Sites | 2 m | 4 m | 8 m |
|-------|-----|-----|-----|
| VY | 0.037–0.038 | 0.057–0.085 | 0.140–0.160 |
| VI | 0.068 | 0.105 | 0.198 |
| VM | 0.062–0.094 | 0.095–0.155 | 0.235–0.330 |
| Mnb | 0.200–0.210 | 0.37–0.42 | 0.660–0.720 |
| ChY | 0.066–0.105 | 0.130–0.155 | 0.202–0.206 |
| ChM | 0.110–0.125 | 0.245–0.280 | 0.435–0.480 |

[a]The tree types are the three ages of planted poplar at Verdun (VY, VI, and VM), the Monbequi natural poplar site (Mnb), and the two different aged natural poplars at Chatel        nd ChM).

**Table 8.** Manning's *n* Values for Flow in Natural Vegetation[a]

| Areas Described | Manning's *n* Range | Source |
|-----------------|---------------------|--------|
| Heavy stand with flow below the branches | 0.080–0.120 | *Chow* [1959] |
| Heavy stand with flow in the branches | 0.100–0.160 | *Chow* [1959] |
| Natural forests with flooding below canopy, winter | 0.065–0.140 | *Arcement and Schneider* [1989] |
| Natural forests with flooding in early canopy, winter | 0.120–0.200 | *Arcement and Schneider* [1989] |

[a]The first two areas described are relevant also to summer flows.
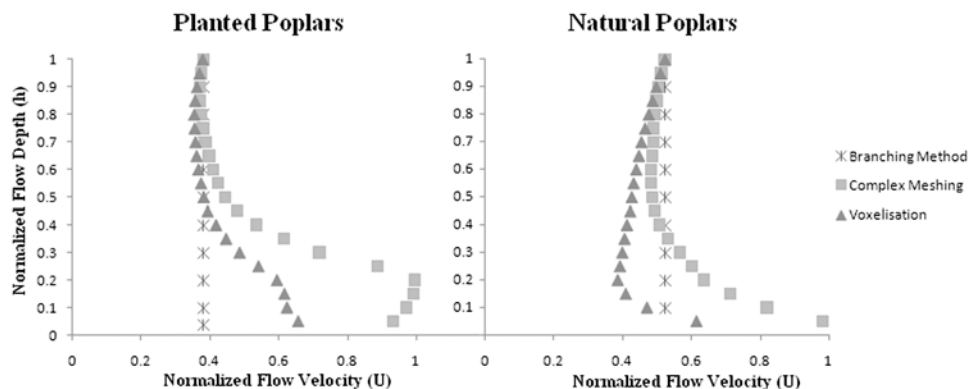
**Figure 7.** Normalized flow velocity distributions calculated for an increase in the normalized flow depth for the methods described in this study (complex meshing, voxel creations, and branching method) and for the two main forest types (planted and natural). The flow velocities are normalized for easier comparison between methods and forest types. The branching method assumes linear increase of projected area with height.

and between the different forest structures. Figure 7 shows the normalized velocity distribution between the two TLS methods and the branching method for the planted and natural forest stands.

[44] It is expected that for planted poplars (as illustrated in Figure 7), or for all trees that typically have a clear separation of the crown from the ground, that flow velocity will be high and steady or growing in magnitude until the flood stage enters the crown level. In fact the complex meshing TLS method has resulted in increasing velocities with an increase in trunk height. Once the flow enters the crown, because of the large increase in bark area or blockage to the flow, it is expected that the flow velocity will decrease dramatically. Further up the canopy, the projected tree area may begin decreasing with an in increase in flow depth, and along with the increase in stream power, results in an increase in flow velocities. Natural poplars, or trees that have their crown near the ground, lack the naked trunk layer, resulting in flow velocities that rapidly decrease from the lowest flow depths.

[45] Few studies have been able to experimentally derive velocity profiles for real trees, and have resorted to modeling or flume techniques. For example, *Yagci and Kabdalsi* [2008] illustrated velocity profiles of two types of vegetation (*Pinus pinea* and *Thuja orientalis*) using flume studies and calculations. *Pinus pinea* represents a species that generally has a larger trunk height than *Thuja orientalis*. Their results did not represent the full submergence of the represented tree, but still they form a good comparison to the velocity profiles in Figure 7. The results from their study demonstrated an increase in flow velocity near the ground through the *Pinus pinea* (potentially representing the trunk), while flow through *Thuja orientalis* almost immediately demonstrated a decrease in velocity (representing a lower crown height). *Yang et al.* [2007] also performed flume experiments over eight structural tree types until full submergence. Their results for all trees showed stark similarities between lower, middle and upper levels of flow velocity around the submerged vegetation, to Figure 7, with similar points of inflection in the velocity profile curves. *Chester et al.* [2007] modeled the velocity in and around a simple tree structure with       trunk (i.e., crown not near

the ground). Their three-dimensional flow velocities resulting from flow around a model tree exhibited high velocities around the trunk, with a marked decrease in velocity around the crown, and finally an increase in velocity near the top of the canopy.

## 7. Conclusions

[46] The first and last pulse airborne lidar data are insufficient to characterize the complex vertical structure of vegetation, because there are few data at intermediate levels. Therefore, terrestrial laser scanning has been used in this study to define complex canopy structures at a millimeter resolution for the purpose of parameterizing roughness in resistance equations considering flow in bare canopies. Comparatively, the total projected areas determined empirically from the Branching Method defined by *Järvelä* [2004] were similar to the Complex Mesh and Voxel methods. Thus total projected areas can adequately be defined mainly from field data. Yet, the stage-dependent projected areas were difficult to define solely from field data. Therefore, terrestrial laser scanning was very useful in both determining the total projected areas of the forested vegetation, and determining the projected area with an increase in flow depth. Resulting leafless woody vegetation roughness values for both planted and natural forests fell within the range defined by the guideline literature. This was true only of the first couple of meters of flow depth, as little to no data are available for flow that enters that intermediate to high levels of the canopy because of the rarity of this event and prior difficulty in acquiring measurements. Roughness values for planted poplars ranged from $n = 0.037 - 0.094$ and $n = 0.140 - 0.330$ for below-canopy flow (2 m) and extreme in-canopy flow (8 m), respectively. Roughness values for natural poplars ranged from $n = 0.066 - 0.210$ and $n = 0.202 - 0.720$ for below-canopy flow (2 m) and extreme in-canopy flow (8 m), respectively. The site with the highest roughness values was the Monbequi site, which offered around 1.25 times more resistance that the other mature natural poplar forests at Chatel. This can be primarily explained by the density of the vegetation elements due to their high competition in the riparian zone.

[47] For the methods presented in this study, all have their limitations and assumptions. The biggest issue with the methods derived from the ground scanning data was not the quality of the point positioning accuracy, but a combination of two factors. The first was the effect of the wind on the scanning of the branches, and the second was the points reflected from the edges of objects (such as the edges of cylindrical branches). For the branching ratio method, the most sensitive parameter was the diameter ratio as described by *Järvelä* [2004], as changing this parameter could alter the friction factor $f$ by +26 to $-18\%$. However, the lengths and length ratios were more difficult to define than the diameter ratio, so it is fortunate that they could be compared to the $R_D$ value.

[48] This study has focused on extracting the projected area from the six tree types. The complex meshing and voxelizing methodologies to determine the projected area have been semiautomated with the help of intensive programming to deal with an enormous number of points in such a dense and small area. This work first introduces the need to produce fully automated techniques that not only extract projected areas, but also branch parameters. This may be very difficult in practice, especially when dealing with huge volumes of data. This research also demonstrates the ability of terrestrial scanning in ideal conditions to work together with ground truthing to extract meaningful information of branch characteristics. These ideal conditions consider accurate recording of points from a stable tree, with an optimum coverage of all the branches and bark of the tree.

[49] Data and research on vegetation characteristics and resistance parameterization are rare. An increase in knowledge about simple and complex canopy roughness for various types of vegetation is necessary, especially when considering overall roughness inputs both lumped and distributed in hydraulic modeling. This research even offers resistance values for extreme flood events when flow is deep and interacts with the canopy. The limit to the parameterization of roughness could even be defined as the limit of resistance equations offering information on multiple interactions of water with canopies, and simultaneously with the understory. Further research has been done to deal with the next level of complexity in vegetation roughness, and parameterizes roughness when the leaves of canopies are included. Again, terrestrial laser scanning is used as well as other information such as multispectral satellite data.

[50] This study finally touches on the subject of extreme flooding events, with roughness values associated with flow depths deep into forest canopies. It has been widely stated that the flood related consequences of climate change will be serious, and the magnitude of events and extent of flooding may be larger. A lot of research has thus focused on trying to predict the probability of extreme flood events in a regional climatic zone, or in specific river basins. Little research has focused on quantifying the hydraulic effects of such floods, and especially of their spatial spread across the floodplain. Hydraulic modeling can be used as a major tool in order to extract information on regional floodwater extents, local discharge and velocity vectors, increases in stream power and erosion, and so on. At the first and second dimension of hydraulic modeling (regional scale), extract-

ing these results in forested floodplains is limited by the capability to ascertain the resistance associated with forests at different levels of flow depth. In 3-D hydraulic modeling (local scale), extracting meaningful results in forested areas is limited by how the boundary conditions are set in terms of the physical forest objects. Therefore, this study provides both the techniques to calculate forest roughness at high flow depths, and to construct a physical forest.

## References

Antonarakis, A. S., K. S. Richards, J. Brasington, M. Bithell, and E. Muller (2008a), Retrieval of vegetative fluid resistance terms for rigid stems using airborne lidar, *J. Geophys. Res.*, 113, G02S07, doi:10.1029/2007JG000543.

Antonarakis, A. S., K. S. Richards, and J. Brasington (2008b), Object-based land cover classification using airborne lidar, *Remote Sens. Environ.*, 112(6), 2988–2998, doi:10.1016/j.rse.2008.02.004.

Arcement, G. J., Jr., and V. R. Schneider (1989), Guide for selecting Manning's roughness coefficients for natural channels and flood plains, *U.S. Geol. Surv. Water Supply Pap., 2339*.

Barker, S. B., G. Cumming, and K. Horsfield (1973), Quantitative morphometry of branching structure of trees, *J. Theor. Biol.*, 40(1), 33–43, doi:10.1016/0022-5193(73)90163-X.

Chester, S., C. Meneveau, and M. B. Parlange (2007), Modeling turbulent flow over fractal trees with renormalized numerical simulation, *J. Comput. Phys.*, 225(1), 427–448, doi:10.1016/j.jcp.2006.12.009.

Chow, V. Y. (1959), *Open Channel Hydraulics*, McGraw-Hill, New York.

Coon, W. F. (1997), Estimation of roughness coefficients for natural stream channels with vegetated banks, *U.S. Geol. Surv. Water Supply Pap., 2441*, 133 pp.

Fathi-Maghadam, M., and N. Kouwen (1997), Nonrigid, nonsubmerged, vegetative roughness on floodplains, *J. Hydraul. Eng.*, 123(1), 51–57, doi:10.1061/(ASCE)0733-9429(1997)123:1(51).

Fleurant, C., J. Duchesne, and P. Raimbault (2004), An allometric model for trees, *J. Theor. Biol.*, 227(1), 137–147, doi:10.1016/j.jtbi.2003.10.014.

Frei, E., J. Kung, and R. Bukowski (2005), High definition surveying (HDS): A new era in reality capture, *Int. Arch. Photogramm. Remote Sens. Spatial Inf. Sci.*, 36, 204–208.

Gorte, B., and N. Pfeifer (2004), Structuring laser-scanned trees using 3D mathematical morphology, *Int. Arch. Photogramm. Remote Sens.*, 35, 929–933.

Gorte, B., and D. Winterhalder (2004), Reconstruction of laser-scanned trees using filter operations in the 3D raster domain, *Int. Arch. Photogramm. Remote Sens. Spatial Inf. Sci.*, 36, 39–44.

Horman, K., and M. Reimers (2004), Triangulating point clouds with spherical topology, in *Curve and Surface Fitting: Saint-Malo 2002*, edited by A. Cohen, J.-L. Merrien, and L. L. Shumaker, pp. 215–225, Nashboro, Brentwood, Tenn.

Hosoi, F., and K. Omasa (2006), Voxel-based 3-D modeling of individual trees for estimating leaf area density using high-resolution portable scanning lidar, *IEEE Trans. Geosci. Remote Sens.*, 44(12), 3610–3618, doi:10.1109/TGRS.2006.881743.

Ishikawa, H., S. Amano, and K. Yakushiji (2006), Flow around a living tree, *JSME Int. J., Ser. B*, 49(4), 1064–1069, doi:10.1299/jsmeb.49.1064.

Järvelä, J. (2002), Flow resistance of flexible and stiff vegetation: A flume study with natural plants, *J. Hydrol.*, 269(1–2), 44–54, doi:10.1016/S0022-1694(02)00193-2.

Järvelä, J. (2004), Determination of flow resistance caused by non-submerged woody vegetation, *Int. J. River Basin Manage.*, 2(1), 61–70.

Kim, S. I., and R. X. Li (2006), Complete 3D surface reconstruction from unstructured point cloud, *J. Mech. Sci. Technol.*, 20(12), 2034–2042, doi:10.1007/BF02916320.

Kouwen, N., and M. Fathi-Moghadam (2000), Friction factors for coniferous trees along rivers, *J. Hydraul. Eng.*, 95(2), 329–342.

Lee, J. K., L. C. Roig, H. L. Jenter, and H. M. Visser (2004), Drag coefficients for modeling flow through emergent vegetation in the Florida Everglades, *Ecol. Eng.*, *22*, 237–248, doi:10.1016/j.ecoleng.2004.05.001.

McMahon, T. A., and R. E. Kronauer (1976), Tree structures: Deducing the principle of mechanical design, *J. Theor. Biol.*, *59*, 443–466, doi:10.1016/0022-5193(76)90182-X.

Muller, E., H. Guilloy-Froget, N. Barsoum, and L. Brocheton (2002), *Populus nigra* L. en vallée de Garonne: Legs du passé et constraints du présents, *C. R. Biol.*, *325*, 1129–1141, doi:10.1016/S1631-0691(02)01519-6.

Oohata, S., and T. Shidei (1971), Studies on the branching structure of trees I. Bifurcation ratio of trees in Horton's law, *Jpn. J. Ecol.*, *21*, 7–14.

Pasche, E., and G. Rouvé (1985), Overbank flow with vegetatively roughened flood plains, *J. Hydraul. Eng.*, *111*(9), 1262–1278, doi:10.1061/(ASCE)0733-9429(1985)111:9(1262).

Remondino, F. (2003), From point cloud to surface: The modelling and visualisation problem, *Int. Arch. Photogramm. Remote Sens. Spatial Inf. Sci.*, *34*, 1–11.

Steingraeber, D. A., J. J. Kascht, and D. H. Franck (1979), Variation of shoot morphology of bifurcation ratio in sugar maple saplings, *Am. J. Bot.*, *66*, 441–445, doi:10.2307/2442397.

Stoker, J. M. (2004), Voxels as a representation of multiple-return lidar data, paper presented at Annual Conference, Am. Soc. for Photogramm. Remote Sens., Denver, Colo.

Strahler, A. N. (1956), The nature of induced erosion and aggradation, in *Man's Role in Changing the Face of the Earth*, edited by W. L. Thomas, pp. 621–638, Univ. of Chicago Press, Chicago, Ill.

Tsihrintzis, V. A. (2001), Variation of roughness coefficients for unsubmerged and submerged vegetation, *J. Hydraul. Eng.*, *127*(3), 241–245, doi:10.1061/(ASCE)0733-9429(2001)127:3(241).

Wu, F. C., H. W. Shen, and W. J. Chou (1999), Variation of roughness coefficients for unsubmerged and submerged vegetation, *J. Hydraul. Eng.*, *125*(9), 934–942, doi:10.1061/(ASCE)0733-9429(1999)125:9(934).

Yagci, O., and M. S. Kabdalsi (2008), The impact of single natural vegetation elements on flow characteristics, *Hydrol. Processes*, *22*, 4310–4321, doi:10.1002/hyp.7018.

Yang, K., C. Shuyou, and D. W. Knight (2007), Flow patterns in compound channels with vegetated floodplains, *J. Hydraul. Eng.*, *133*(2), 148–159, doi:10.1061/(ASCE)0733-9429(2007)133:2(148).

————————————

A. S. Antonarakis, Department of Organismic and Evolutionary Biology, Harvard University, 26 Oxford Street, Cambridge, MA 02138, USA. (aantonarakis@oeb.harvard.edu)

M. Bithell and K. S. Richards, Department of Geography, University of Cambridge, Downing Place, Cambridge CB2 3EN, UK.

J. Brasington, Institute of Geography and Earth Sciences, University of Wales, Llandinam Building, Penglais Campus, Aberystwyth SY23 3DB, UK.